Available online at www.sciencedirect.com
SCIENCE DIRECT®
Computers and Electronics in Agriculture 53 (2006) 60–70
Computers and electronics in agriculture
www.elsevier.com/locate/compag

Near-infrared hyperspectral reflectance imaging for detection of bruises on pickling cucumbers

Diwan P. Ariana [a,*], Renfu Lu [a], Daniel E. Guyer [b]

[a] *Sugarbeet and Bean Research Unit, USDA Agricultural Research Service, 224 Farrall Hall, Michigan State University, East Lansing, MI 48824, USA*
[b] *Biosystems and Agricultural Engineering Department, Michigan State University, 211 Farrall Hall, East Lansing, MI 48824, USA*

Received 29 December 2005; accepted 5 April 2006

Abstract

Mechanical injury often causes hidden internal damage to pickling cucumbers, which lowers the quality of pickled products and can incur economic losses to the processor. A near-infrared hyperspectral imaging system was developed to capture hyperspectral images from pickling cucumbers in the spectral region of 900–1700 nm. The system consisted of an imaging spectrograph attached to an InGaAs camera with line-light fiber bundles as an illumination source. Hyperspectral images were taken from the pickling cucumbers at 0–3, and 6 days after they were subjected to dropping or rolling under load which simulated damage caused by mechanical harvesting and handling systems. Principal component analysis (PCA), band ratio, and band difference were applied in the image processing to segregate bruised cucumbers from normal cucumbers. Bruised tissue had consistently lower reflectance than normal tissue and the former increased over time. Best detection accuracies from the PCA were achieved when a bandwidth of 8.8 nm and the spectral region of 950–1350 nm were selected. The detection accuracies from the PCA decreased from 95 to 75% over the period of 6 days after bruising, which was attributed to the self-healing of the bruised tissue after mechanical injury. The best band ratio of 988 and 1085 nm had detection accuracies between 93 and 82%, whereas the best band difference of 1346 and 1425 nm had accuracies between 89 and 84%. The general classification performance analysis suggested that the band ratio and difference methods had similar performance, but they were better than the PCA.

Keywords: Cucumbers; Bruises; Defects; Hyperspectral imaging; Near-infrared

1. Introduction

Excessive mechanical loading or stress during harvest, transport and handling can cause injuries to pickling cucumbers. Severely injured fruit such as broken, smashed, and cuts are easy to identify and can be discarded during the sorting/inspection process. However, mechanical injury often causes hidden internal physical damage to cucumber fruit that is difficult to detect by human inspectors. Internal damage on the affected fruit may cause internal carpel separation which can lead to increased bloating in brine-stock cucumbers (Heldman et al., 1976; Marshall et al., 1972). Bloating of cucumbers during brining represents a major economic loss to pickle processors (Ennis and O'Sullivan, 1979).

* Correspondence to: 105AA Farrall Hall, Michigan State University, East Lansing, MI 48824, USA. Tel.: +1 517 432 8062; fax: +1 517 432 2892.
E-mail address: arianadi@msu.edu (D.P. Ariana).

0168-1699/$ – see front matter © 2006 Elsevier B.V. All rights reserved.
doi:10.1016/j.compag.2006.04.001

A number of methods for detecting bruises on cucumber fruit have been researched. For instance, a catechol test coupled with hydrogen peroxide can be used to detect bruising in whole cucumbers (Hammerschmidt and Marshall, 1991). This test is based on increased peroxidase activity after bruising (Miller and Kelley, 1989). Mechanical injury may result in changes in endogenous levels and rates of biosynthesis of ethylene, indoleacetic acid, zeatin, and elicitors (Miller, 1992), cell wall-degrading enzymes and ethylene production (Miller et al., 1987), and sugar composition of cell wall (Miller, 1989). The aforementioned method is destructive, not instantaneous, and therefore not suitable for automated grading and sorting in a modern commercial setting.

Researchers have explored various nondestructive methods for detecting mechanical injury on cucumber fruit. Sorting cucumbers by density has been proposed because damaged fruit have internal voids and may have different densities than undamaged fruit (Marshall et al., 1973). However, the rate of misclassification by density was high. Refreshed delayed light emission (RDLE) from chlorophyll was able to consistently distinguish bruised from non-bruised cucumber fruit (Abbott et al., 1991) Although the method is impractical for sorting individual pickling cucumbers due to the time requirement for dark equilibrium and RDLE measurement, it has potential to be used as an inspection tool by the processor. Visible/near-infrared light transmission measurement has been studied to evaluate internal quality of pickling cucumbers (Miller et al., 1995). Light transmission increased as the severity of mechanical stress applied to the fruit increased. The technique may be a valuable tool for detecting poor quality cucumbers before processing.

Recently, considerable research has been reported on using hyperspectral imaging for quality and safety inspection of agricultural products, such as bruises and other defects on apples (Lee et al., 2005; Lu, 2003; Lu et al., 1999; Mehl et al., 2004), fecal contamination on apples and poultry carcasses (Kim et al., 2002; Park et al., 2002), and the ripeness of tomatoes (Polder et al., 2002). Hyperspectral imaging has also been studied for detecting chilling injury on cucumbers (Cheng et al., 2004; Liu et al., 2005). Hyperspectral imaging technology currently cannot be directly implemented in an online system for agricultural product sorting because of the extensive time required for image acquisition and subsequent analysis. However, hyperspectral imaging can be a very useful research tool for determining important spectral bands, which later can be implemented in a multispectral imaging system. These spectral bands can be obtained through different analysis methods such as spectral difference and principal component analysis (Liu et al., 2005; Lu, 2003; Mehl et al., 2004).

The objective of the research was to study the potential of hyperspectral imaging in the spectral region between 900 and 1700 nm for detection of bruises on pickling cucumbers. Specific objectives were to:

- develop a near-infrared (NIR) hyperspectral imaging system for fast acquisition of hyperspectral reflectance images from pickling cucumbers;
- develop computer algorithms to identify and segregate bruises from normal tissue of cucumbers; and
- identify the spectral region and/or wavelengths that are most useful for detection of bruises.

2. Materials and methods

2.1. Sample preparation

'Journey' cucumbers were hand harvested from an experimental field of the Horticultural Research and Teaching Center south of Michigan State University's campus in East Lansing, Michigan, USA in August 2005. Ninety commercial size three cucumbers (37–55 mm diameter) that were free from defects and misshaping were selected and randomly subdivided into three groups of 30 cucumbers each. Within 24 h after harvesting, two groups of cucumbers were subjected to bruising by either dropping or rolling under load to simulate stress caused by mechanical harvesting and handling systems. No mechanical stress was applied to the other group. The dropping test was performed by dropping each cucumber from 1 m height onto a tiled floor six times with random radial orientations (Abbott et al., 1991). The rolling test was performed by rolling each cucumber for 1 min between a benchtop and a 30 cm square board supporting a 10 kg mass (Miller et al., 1987).

2.2. Hyperspectral imaging system

A near-infrared hyperspectral imaging system consisting of three major units was developed for the study (Fig. 1). The imaging unit had an InGaAs area array camera (Model SU320MX-1.7RT, Sensors Unlimited, Princeton, NJ,

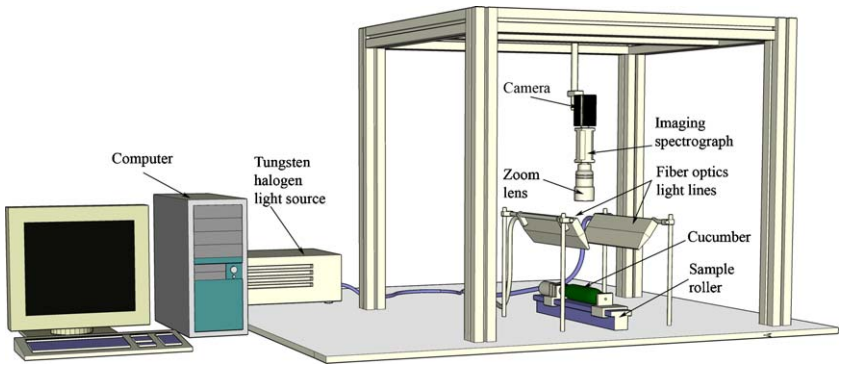

Fig. 1. Near-infrared hyperspectral imaging system.

USA) covering the spectral range between 900 and 1700 nm, an imaging spectrograph (Model ImSpector N17E, Specim, Finland) attached to the camera, a zoom lens (Model Zoom 7000, Navitar Inc., Rochester, NY, USA), and a frame grabber (Model IMAQ PCI-1422, National Instrument, Austin, TX, USA) attached to a PCI bus of a Pentium 4 computer for controlling the camera and acquiring image data. The lighting unit was a DC regulated light source from a 150 W tungsten halogen lamp (Model FTIII16797-RS232, Fiberoptics Technology Inc., Pomfret, CT, USA) delivered through dual fiber optic light lines (Model FTIDL16855-6, Fiberoptics Technology Inc., Pomfret, CT, USA). The third unit was a specially designed sample roller for positioning the fruit for imaging. The InGaAs camera had an area array of 320 × 240 pixels and the quantum efficiency greater than 70% over the specified spectral region. The imaging spectrograph, with a slit size of 80 μm and an F-number of 2.0, scanned the fruit one line a time. The spectral resolution of the system was 4.4 nm. The field of view of the zoom lens was set to approximately 110 mm as the length of the scan line, only covering the cucumber sample without including the background scene. The hyperspectral imaging unit was pre-calibrated both spatially and spectrally by following the procedure described in Lu and Chen (1998) and Lawrence et al. (2003).

The cucumber sample was held at both ends by two cone-shaped holders. The distance between the two holders was adjustable to accommodate different lengths of cucumber samples. One of the holder's shafts was connected to a stepper motor controlled by a Basic Stamp microcontroller (Model BS2SX, Parallax Inc., Rocklin, CA, USA) to rotate the cucumber sample. A computer program was written in C++ to control the camera for acquiring images and to synchronize the rotational speed of the sample.

2.3. Image acquisition

For individual cucumber samples, 100 hyperspectral images that spanned the entire surface of the cucumber were acquired by rotating the cucumber 360° at a speed of 1 rpm. Thus, for each cucumber sample the size of the hyperspectral image cube was 320 × 240 × 100 data points. The spatial resolution of the hyperspectral imaging system was 0.34 mm along the longitudinal direction and 1.03 mm along the circumferential direction.

A first set of hyperspectral images were acquired from the 90 fresh cucumber samples before they were subjected to mechanical stress (i.e., dropping and rolling). Within 2 h after mechanical stress treatment was applied to the assigned cucumbers, the second set of hyperspectral images was taken from each fruit. The cucumbers were imaged again at 1–3, and 6 days after the application of mechanical stress. At the beginning of imaging on each group of 15 cucumbers, hyperspectral images from a 1 in. diameter white Teflon cylinder were also collected. These images were used as a reference to correct the sample images.

2.4. Hyperspectral image analysis

Hyperspectral images of the cucumbers were corrected by the ones from the Teflon cylinder to obtain relative reflectance images using the following equation:

$$R_c = \frac{I_s - I_d}{I_r - I_d} \quad (1)$$

where R_c is the relative reflectance image, I_s the sample image, I_r the reference image from the Teflon cylinder, and I_d is the dark image. Due to low efficiencies of the system at both ends of the 900–1700 nm spectrum, only the wavelength range from 950 to 1650 nm was used for analysis.

In order to determine the effectiveness of the bruise detection algorithm, it was necessary to have advanced knowledge about bruises and their locations on individual cucumber samples. The actual individual cucumber class (bruised or normal) was determined by visually comparing relative reflectance NIR images at 1200 nm before and after mechanical stress was applied. Bruised areas appeared as dark patches in the NIR images. Bruised and normal areas had highest contrast at 1200 nm. If dark areas appeared only on the NIR images after bruising, the cucumber was designated to be the bruised class. Rough skin areas, which appeared as dark areas on both NIR images before and after bruising, were not considered as bruised. In addition to images comparison, visual inspection to the bruised cucumbers, characterized by the presence of water-soaked lesions on the cucumber surface, was also performed after each imaging test to confirm whether each cucumber was bruised.

Regions of interest (ROIs) representing both normal and bruised areas were selected manually from individual bruised cucumber images at 1200 nm using a polygonal region of interest function in MATLAB (The Math Works Inc., Natick, MA, USA). The ROIs for bruised areas were selected from the dark areas that appeared only in the images after bruising, whereas normal areas were selected from light smooth areas in the image. ROI sizes varied from 12 to 1343 pixels for bruised cucumbers and from 64 to 1566 pixels for normal cucumbers. Pixels from the ROIs were analyzed to calculate the mean spectra of the bruised and normal areas. Furthermore, correlation analysis of these pixels was performed to find the maximum correlation coefficient for the ratio or difference of reflectance at two wavelengths. To calculate the correlation coefficient, the quality index value of 1 or 0 was assigned to pixels from bruised and normal areas, respectively. An optimal threshold value was chosen to segregate the bruised areas from normal areas of ratio and difference images of selected wavelengths.

Principal component analysis (PCA) on the corrected hyperspectral images [Eq. (1)] was performed to reduce spectral dimensionality and enhance image features. Due to the large size of hyperspectral images, it is desirable to find an optimal bandwidth in order to minimize the amount of data to be processed without sacrificing detection results. To find the optimal bandwidth, principal components were computed based on the original spectral resolution (4.4 nm) with 160 wavebands and reduced spectral resolutions (by binning process) of 8.8, 17.6, and 35.2 nm with the corresponding 80, 40, and 20 wavebands. Principal components based on the optimal bandwidth were also computed for each of the three spectral regions (950–1650 nm, 950–1350 nm, and 1150–1350 nm). The relations among these components for the bruised and normal areas were explored using scatter plots. An optimal threshold value was chosen to segregate bruised from normal areas based on the principal component images.

The receiver operating characteristic (ROC) curve is a way of visualizing a classifier's performance in order to select a suitable operating point, or decision threshold. The area under the ROC curve (AUC) is a measure of classifier's performance, and it is useful for comparing a number of different classification schemes (Bradley, 1997). ROC curves were created from a range of threshold values. The area under the ROC curve was used to compare the overall performance of the three classification methods: band ratio, band difference, and principal components. An optimal threshold value was chosen from a point in the ROC curve which is the closest point to the top left corner of the curve (where the true positive rate equals 1 and the false positive rate equals 0). A segmented cucumber image at a selected threshold value from the corresponding processed images (band ratio, band difference, or first principal component) was classified as bruised if it contained more than five bruised pixels. Classification accuracy calculation was based on the percentage of correctly classified segmented images as bruised or normal cucumber samples.

MATLAB programs using Image Processing and Statistics Toolbox were written and used for performing principal component analysis of the hyperspectral images, image segmentation, and image classification.

3. Results and discussion

3.1. Spectral characteristics of bruised and normal tissue

Fig. 2 shows the mean reflectance spectra of normal and bruised cucumber tissue in the region of 950–1650 nm. The mean spectra were calculated based on pixels of the ROIs from all cucumber samples over the period of 0–6 days after mechanical stress. The mean reflectance of bruised tissue was consistently lower than that from the normal tissue

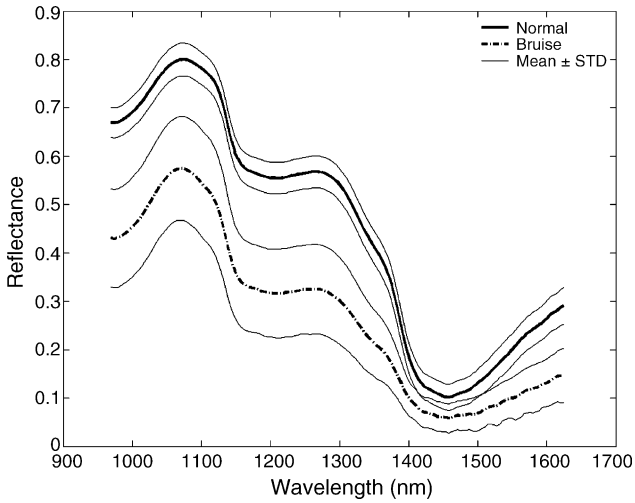

Fig. 2. Mean relative reflectance spectra of normal and bruised cucumber tissue and their standard deviation (S.D.) spectra.

over the entire spectral region, except in the range of 1400–1500 nm where considerable spectral overlapping was observed for the two types of tissue. Water has strong absorption at 1450 nm (Osborne et al., 1993), which resulted in low reflectance for both normal and bruised tissue (Fig. 2).

The difference in the reflectance between normal and bruised tissue was greatest in the region between 950 and 1350 nm. The reflectance of normal tissue was relatively constant over the period of the experiment. On the contrary, the reflectance of bruised tissue increased over time, approaching that of normal tissue (Fig. 3). This characteristic might be due to the wound healing of the cucumbers in response to mechanical stress (Miller, 1992). Fig. 4 shows the changes in bruised areas with time from the spectral images at 1200 nm taken over a period of 6 days. Within 2 h after bruising (0 day), bruises appeared darker than normal tissue on the image. One day after stress was applied, the relative reflectance of bruised tissue showed the greatest difference from that of normal tissue. This fact is an advantage for machine vision-based sorting because freshly harvested cucumbers are usually sorted within 24 h after harvesting. The spectral differences between the bruised and normal tissue decreased over time. Some bruise areas were no longer visible on the image after 6 days. Thus, sorting at later days is not desirable.

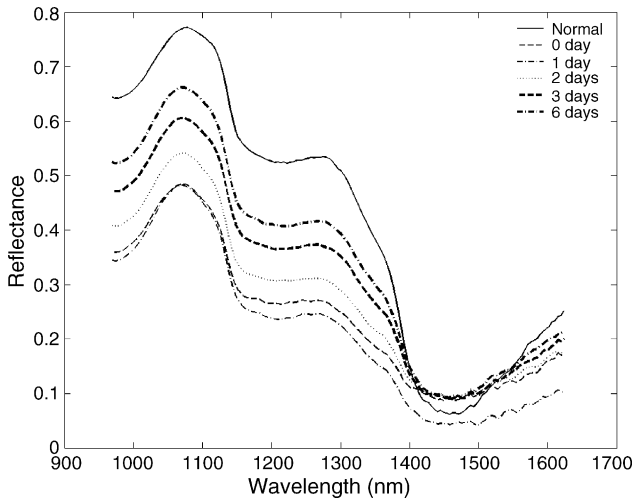

Fig. 3. Mean relative reflectance changes on bruised tissue of the cucumbers over periods 0–6 days after mechanical stress.

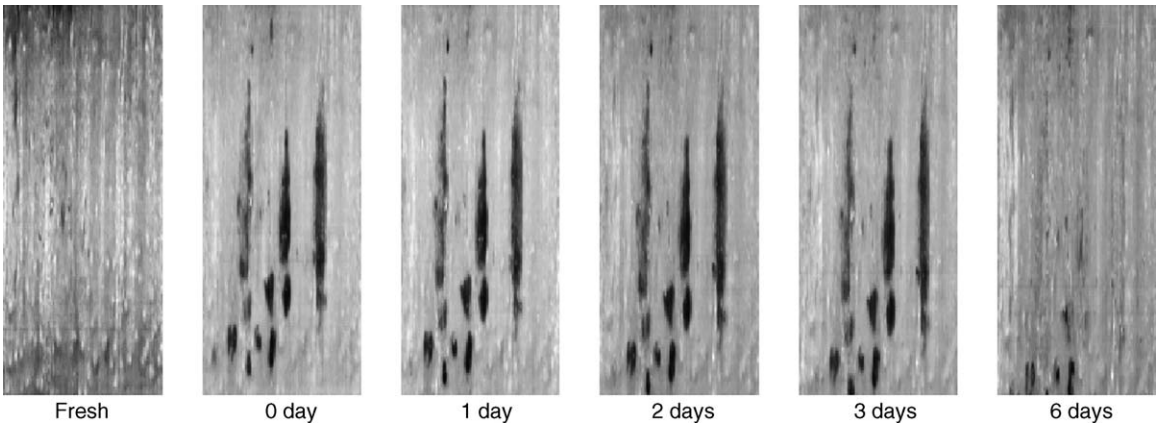

Fig. 4. Near-infrared spectral images at 1200 nm showing the changes in bruises over time periods 0–6 days.

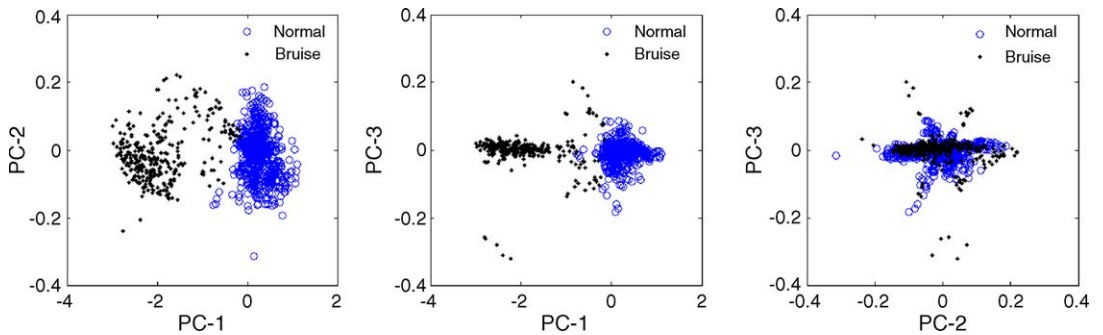

Fig. 5. Scatter plots of the first three principal components of near-infrared hyperspectral images over the spectral region 950–1350 nm.

3.2. Principal component analysis

The first principal component covered around 90% of the image variation across the wavebands. The first principal component images possibly represented the mean of hyperspectral images over a spectral region, as they appeared similar to the spectral images at individual wavelengths. The ROIs of bruised and normal areas from the first principal component were determined. The same ROIs were applied to the second and third component. The scatter plots of pixels from these ROIs are shown in Fig. 5. Two separate clusters of bruised and normal tissue were observed from the scatter plots of PC-1 versus PC-2 and PC-1 versus PC-3. The scatter plots show that the two groups of tissue were clearly distinguishable along the PC-1 axes. Therefore, the first principal component alone was sufficient to distinguish the bruised tissue from normal tissue.

The classification accuracies based on the first principal components obtained from different spectral resolution data are shown in Table 1. The table indicates that the spectral resolution of 8.8 nm resulted in the best classification

Table 1
Comparison of classification accuracies (in %) based on first principal components over the spectral region of 950–1650 nm obtained from different spectral resolution

Spectral resolution (band numbers)	Days after bruising				
	0	1	2	3	6
4.4 nm (160)	90.9	85.5	85.5	78.2	72.7
8.8 nm (80)	94.6	89.1	89.1	83.6	70.9
17.6 nm (40)	92.7	89.1	87.3	81.8	67.3
35.2 nm (20)	89.1	80.0	76.4	70.9	65.5

Table 2
Classification accuracies (in %) based on first principal components of near-infrared hyperspectral images with spectral resolution of 8.8 nm

Spectral region (nm)	Days after bruising				
	0	1	2	3	6
950–1650	94.6	89.1	89.1	83.6	70.9
950–1350	94.6	92.7	90.9	85.5	74.6
1150–1350	83.6	83.6	85.5	81.8	72.7

accuracies over the period of 0–6 days after bruising. The classification accuracies tend to decrease as the number of bands reduced (wider spectral bandwidth). The results from the original spectral resolution of 4.4 nm were not as good as those obtained from 8.8 to 17.6 nm. These findings are in agreement with those for apples (Lu, 2003). Hence, further analyses to find optimum spectral region and key wavelengths were based on the spectral resolution of 8.8 nm. Higher spectral resolution does not necessarily yield higher detection accuracies. Waveband binning which reduced spectral resolution improved the image quality by increasing the signal-to-noise ratio (Lu, 2003).

Principal components of NIR hyperspectral images based on the optimum spectral resolution 8.8 nm were analyzed in three different spectral regions, 950–1650 nm, 950–1350 nm, and 1150–1350 nm. Table 2 shows the classification accuracies of cucumber samples based on the first principal components over the period of 0–6 days. The best classification accuracies were achieved under the spectral region of 950–1350 nm for all days after mechanical stress. This region represented wavebands where reflectance difference between normal and bruised tissue was greatest. The classification accuracy within 2 h of bruising was 94.6% and decreased over time to 74.6% at day 6 after bruising. Decreasing classification accuracy over time was also observed at the other two regions. This pattern was due to the decreased differences in reflectance between bruised and normal tissue.

3.3. Ratio and difference of two wavelengths

Although only one component was used in the classification, the computation of the principal component included all spectral images for a spectral region. For real time applications, it is more desirable to use fewer (two or three) wavelengths in order to accelerate the image acquisition and analysis process. Analysis of single wavelength classification was not performed in this study because the spectral overlapping between bruised and normal tissue become more apparent over time. This can be clearly seen from Figs. 2 to 3 if the envelope of two standard deviations which only covers 95% of the data is applied.

Ratio or difference of two wavelengths followed by image segmentations using a threshold was used in this study. Park et al. (2005) used band ratio of two wavelengths, which were selected based on the reflectance spectra obtained from hyperspectral images, for detecting cecal contaminants in the visceral cavity of broiler carcasses. The best two wavelengths for the ratio and difference algorithm were found using correlation analysis of all possible wavelengths. For the ratio of two wavelengths, the best wavelengths are 988 and 1085 nm, as calculated by Eq. (2):

$$R = \frac{R_{988\,\mathrm{nm}}}{R_{1085\,\mathrm{nm}}} \tag{2}$$

where $R_{988\,\mathrm{nm}}$ and $R_{1085\,\mathrm{nm}}$ are relative reflectance at 988 and 1085 nm, respectively.

Wavelengths 1346 and 1425 nm were found to be the best for difference calculations:

$$D = R_{1346\,\mathrm{nm}} - R_{1425\,\mathrm{nm}} \tag{3}$$

where $R_{1346\,\mathrm{nm}}$ and $R_{1425\,\mathrm{nm}}$ are relative reflectance at 1346 and 1425 nm, respectively.

Classification performances based on R and D images are shown in Figs. 6 and 7, respectively. The performances are presented in the forms of the receiver operating characteristic (ROC) curve and classification accuracy curve. The ROC curves were generated from a range of threshold values where the distribution of R and D values for bruised and normal tissue overlapped. In a classification task there is always a compromise between choosing a high true positive rate (the ability to detect bruises) and keeping a low false positive rate (classify normal as bruise). A closest point in the ROC curve to the top left corner of the chart (where the true positive rate equals 1 and the false positive rate equals 0) generally resulted from an optimal threshold. The threshold values of 0.79 and 0.16 were selected for R and

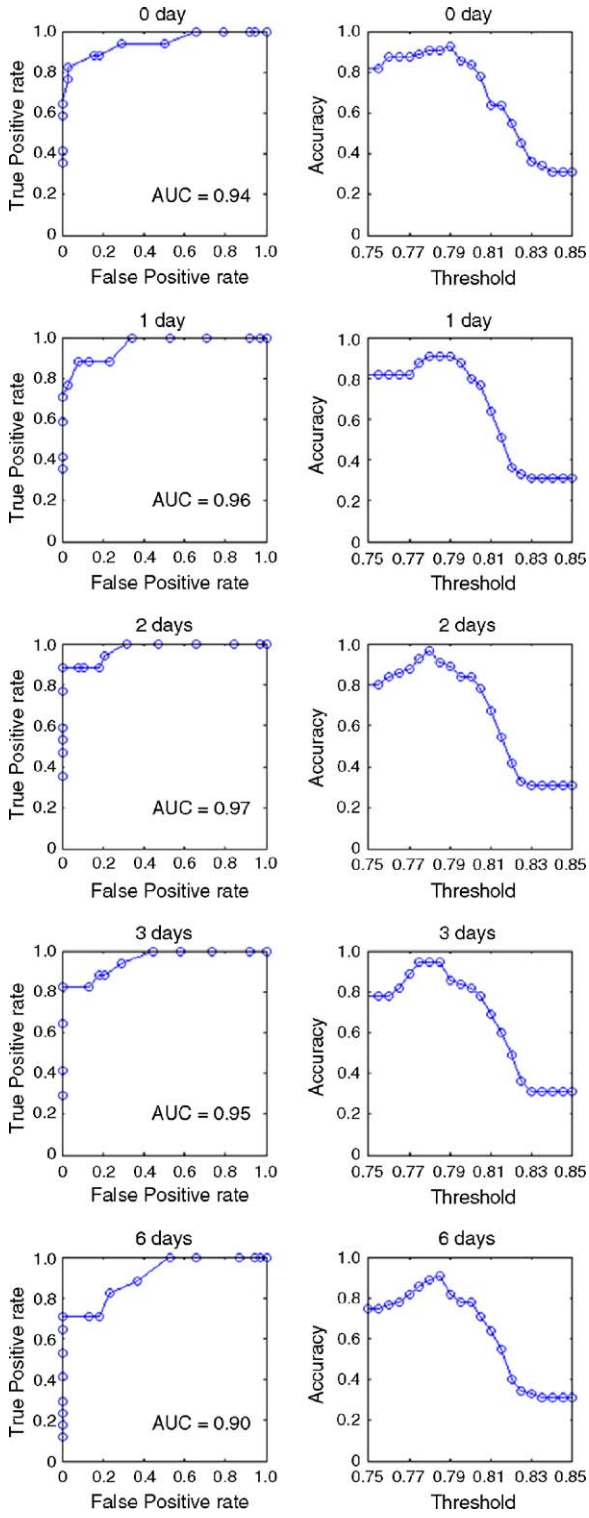

Fig. 6. Classification performances based on the ratio of reflectance (R) images for two wavelengths ($R = R_{988nm}/R_{1085nm}$) over a period of 0–6 days. Left plots: receiver operating characteristics (ROC) curve; right plots: classification accuracy curve (AUC, area under curve).

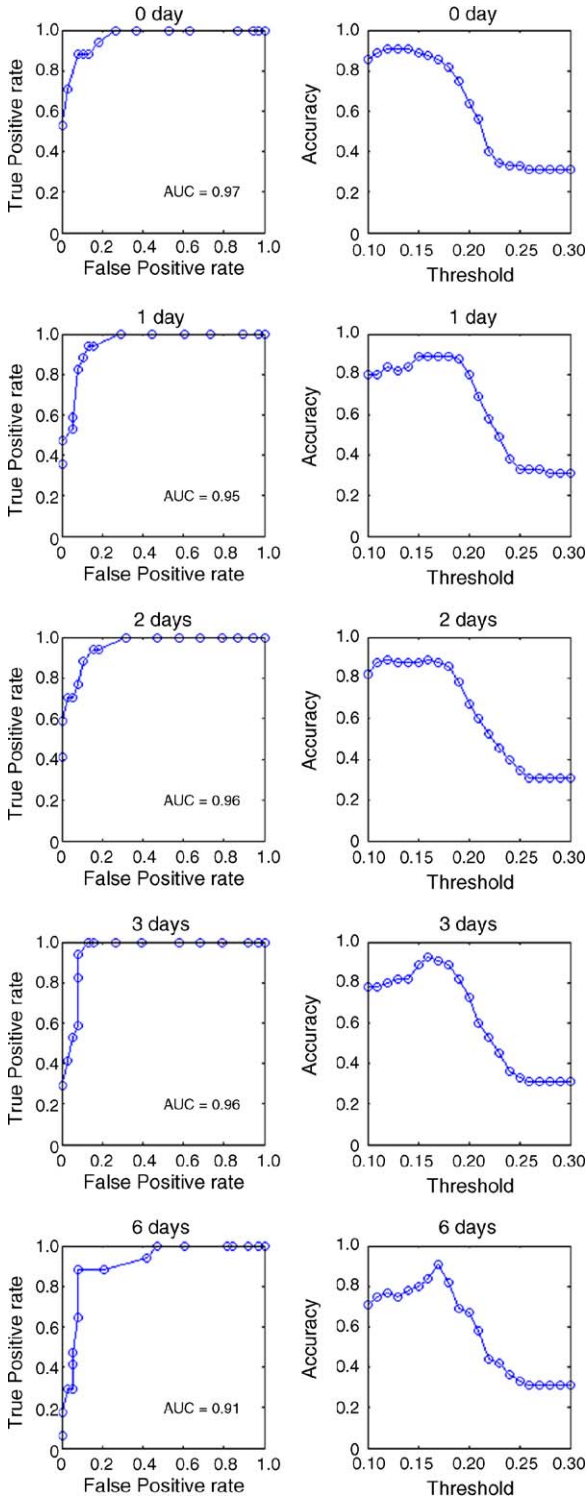

Fig. 7. Classification performances based on the difference of reflectance images for two wavelengths ($D = R_{1346\text{nm}} - R_{1425\text{nm}}$) over a period of 0–6 days. Left plots: receiver operating characteristics (ROC) curve; right plots: classification accuracy curve (AUC, area under curve).

Table 3
Classification accuracies (in %) based on ratio and difference of two near-infrared spectral images

Calculation[a]	Days after bruising				
	0	1	2	3	6
$R = R_{988nm}/R_{1085nm}$	92.7	90.9	89.1	85.5	81.8
$D = R_{1346nm} - R_{1425nm}$	87.3	89.1	89.1	92.7	83.6

[a] R_{988nm}, R_{1085nm}, R_{1346nm}, and R_{1425nm} are relative reflectance images at their respective wavelengths.

D values, respectively, and their accuracies over a period of 0–6 days are shown in Table 3. The classification accuracy based on the ratio of two wavelengths was slightly better than that based on the difference of two wavelengths for 0 and 1 days after bruising, whereas the difference of two wavelengths was superior for 3 and 6 days. Area under the ROC curve (AUC) is often used to compare general classification performances. The AUC has an important statistical property: the AUC of a classifier is equivalent to the probability that the classifier will rank a randomly chosen positive instance higher than a randomly chosen negative instance (DeLong et al., 1988). Based on the AUC comparisons, the classification performance for the band difference method was slightly better than that of band ratio at 0, 3, and 6 days.

Classification based on the first principal component over the region of 950–1650 nm (Table 2) yielded higher accuracies at 0 and 1 day compared to classification based on *R* or *D* values (Table 3). However, its accuracy at 6 days after bruising was much lower than that from band difference or ratio. The general classification performance based on the first principal component was also inferior to that based on the *R* or *D* values. The AUC based on the first principal component under 950–1350 nm region was 0.93, 0.90, 0.90, 0.88, and 0.77 for 0–3, and 6 days, respectively. Classification accuracy based on the first principal component seemed more sensitive to the age of tissue bruising. Hence, the method of band ratio or difference is preferable because their classification accuracy was more stable over time.

4. Conclusions

The reflectance of bruised tissue on cucumber fruit was generally lower than that of normal tissue, and the former increased over time towards that of normal tissue. Consequently, the detection accuracy was also affected by time after bruising. This study found that the spectral region between 950 and 1350 nm with a bandwidth of 8.8 nm was most useful in principal component analysis for bruise detection. The classification accuracies based on bruise segmentations on the first principal component images decreased from 95% at 0 day to 75% at 6 days after bruising. The relatively low performance at later days after bruising may have been caused by the self-healing characteristic of cucumber tissues.

For real-time application, it is desirable to use fewer wavelengths for rapid image acquisition and processing. For the ratio of reflectance images, the best bruise classification accuracy was achieved using 988 and 1085 nm, whereas for the difference of reflectance images, the best classification was obtained using 1346 and 1425 nm. The general classification performance analysis demonstrated that images difference of two wavelengths was better than the ratio of two wavelengths and principal component analysis within 1 day of bruising. The classification accuracies for the ratio of two wavelengths were between 93 and 82%, whereas the accuracies for the difference of two wavelengths were between 89 and 84% for the time period of 0–6 days after bruising.

Acknowledgements

The authors appreciate Mr. Benjamin Bailey, Engineering Technician, for providing technical support to this research. Thanks also go to Dr. Mathieu Ngouajio in the Horticulture Department of Michigan State University for providing cucumber samples.

References

Abbott, J.A., Miller, A.R., Campbell, T.A., 1991. Detection of mechanical injury and physiological breakdown of cucumbers using delayed light emission. J. Am. Soc. Horticult. Sci. 116 (1), 52–57.

Bradley, A.P., 1997. The use of the area under the ROC curve in the evaluation of machine learning algorithms. Pattern Recog. 30 (7), 1145–1159.
Cheng, X., Chen, Y.R., Tao, Y., Wang, C.Y., Kim, M.S., Lefcourt, A.M., 2004. A novel integrated PCA and FLD method on hyperspectral image feature extraction for cucumber chilling damage inspection. Transact. ASAE 47 (4), 1313–1320.
DeLong, E.R., DeLong, D.M., Clarke-Pearson, D.L., 1988. Comparing the areas under two or more correlated receiver operating characteristic curves: a nonparametric approach. Biometrics 44 (3), 837–845.
Ennis, D.M., O'Sullivan, J., 1979. Cucumber quality – a review. J. Food Sci. 44 (1), 186–189, 197.
Hammerschmidt, R., Marshall, D.E., 1991. Potential use of peroxide in external bruise assessment. Proceedings of the Annual Report to the Pickling Cucumber Industry Committee, p. 49.
Heldman, D.R., Borton, L.R., Marshall, D.E., Segerlind, L.J., 1976. Influence of handling on pickling cucumber quality. Transact. ASAE 19 (6), 1194–1196, 1200.
Kim, M.S., Lefcourt, A.M., Chao, K., Chen, Y.R., Kim, I., Chan, D.E., 2002. Multispectral detection of fecal contamination on apples based on hyperspectral imagery. Part I. Application of visible and near-infrared reflectance imaging. Transact. ASAE 45 (6), 2027–2037.
Lawrence, K.C., Park, B., Windham, W.R., Mao, C., 2003. Calibration of a pushbroom hyperspectral imaging system for agricultural inspection. Transact. ASAE 46 (2), 513–521.
Lee, K.J., Kang, S., Kim, M.S., Noh, S.H., 2005. Hyperspectral imaging for detecting defect on apples. ASAE Paper No. 053075, St. Joseph, Michigan.
Liu, Y., Chen, Y.R., Wang, C.Y., Chan, D.E., Kim, M.S., 2005. Development of simple algorithm for detection of chilling injury in cucumbers from visible/near-infrared hyperspectral imaging. Appl. Spectrosc. 59 (1), 78–85.
Lu, R., 2003. Detection of bruises on apples using near-infrared hyperspectral imaging. Transact. ASAE 46 (2), 523–530.
Lu, R., Chen, Y.R., 1998. Hyperspectral imaging for safety inspection of food and agricultural products. Proc. SPIE 3544, 121–133.
Lu, R., Chen, Y.R., Park, B., Choi, K.H., 1999. Hyperspectral imaging for detecting bruises in apples. ASAE Paper No. 013076, St. Joseph, Michigan.
Marshall, D.E., Cargill, B.F., Levin, J.H., 1972. Physical and quality factors of pickling cucumbers as affected by mechanical harvesting. Transact. ASAE 15 (4), 604–608, 612.
Marshall, D.E., Levin, J.H., Heldman, D.R., 1973. Density sorting of green stock cucumbers for brine stock quality. ASAE Paper No. 73-304, St. Joseph, Michigan.
Mehl, P.M., Chen, Y.R., Kim, M.S., Chan, D.E., 2004. Development of hyperspectral imaging technique for detection of apple surface defects and contaminations. J. Food Eng. 61, 67–81.
Miller, A.R., 1989. Mechanical stress-induced changes in sugar composition of cell walls from cucumber fruit tissues. Phytochemistry 28 (2), 389–392.
Miller, A.R., 1992. Physiology, biochemistry and detection of bruising (mechanical stress) of fruits and vegetables. Postharvest News Info. 3, 53N–58N.
Miller, A.R., Dalmasso, J.P., Kretchman, D.W., 1987. Mechanical stress, storage time, and temperature influence cell wall-degrading enzymes, firmness, and ethylene production by cucumbers. J. Am. Soc. Horticult. Sci. 112 (4), 666–671.
Miller, A.R., Kelley, T.J., 1989. Mechanical stress stimulates peroxidase activity in cucumber fruit. HortScience 24 (4), 650–652.
Miller, A.R., Kelley, T.J., White, B.D., 1995. Nondestructive evaluation of pickling cucumbers using visible-infrared light transmission. J. Am. Soc. Horticult. Sci. 120 (6), 1063–1068.
Osborne, B.G., Fearn, T., Hindle, P.H., 1993. Practical NIR Spectroscopy with Applications in Food and Beverage Analysis. Longman Scientific & Technical, Harlow, England.
Park, B., Lawrence, K.C., Windham, W.R., Buhr, R.J., 2002. Hyperspectral imaging for detecting fecal and ingesta contaminants on poultry carcasses. Transact. ASAE 45 (6), 2017–2026.
Park, B., Lawrence, K.C., Windham, W.R., Smith, D.P., 2005. Detection of cecal contaminants in visceral cavity of broiler carcasses using hyperspectral imaging. Appl. Eng. Agricult. 21 (4), 627–635.
Polder, G., Heijden, G.W.A.M., Young, I.T., 2002. Spectral image analysis for measuring ripeness of tomatoes. Transact. ASAE 45 (4), 1155–1161.